



**HAL**  
open science

# Mobilization of DNAPL lenses in heterogeneous aquifers using shear-thinning PEO polymers: Experimental and numerical study

Amir Alamooti, Adil Baigadilov, Idriss Sawadogo, Richard Martel, Dorian Davarzani, Azita Ahmadi-Sénichault, Stéfan Colombano

## ► To cite this version:

Amir Alamooti, Adil Baigadilov, Idriss Sawadogo, Richard Martel, Dorian Davarzani, et al.. Mobilization of DNAPL lenses in heterogeneous aquifers using shear-thinning PEO polymers: Experimental and numerical study. *Water Research*, 2024, 273, pp.122952. 10.1016/j.watres.2024.122952 . hal-04865616

HAL Id: hal-04865616

<https://brgm.hal.science/hal-04865616v1>

Submitted on 6 Jan 2025

**HAL** is a multi-disciplinary open access archive for the deposit and dissemination of scientific research documents, whether they are published or not. The documents may come from teaching and research institutions in France or abroad, or from public or private research centers.



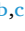

L'archive ouverte pluridisciplinaire **HAL**, est destinée au dépôt et à la diffusion de documents scientifiques de niveau recherche, publiés ou non, émanant des établissements d'enseignement et de recherche français ou étrangers, des laboratoires publics ou privés.



Distributed under a Creative Commons Attribution - NonCommercial 4.0 International License



# Mobilization of DNAPL lenses in heterogeneous aquifers using shear-thinning PEO polymers: Experimental and numerical study

Amir Alamooti<sup>a,b,c,d,\*</sup> , Adil Baigadilov<sup>a</sup>, Idriss Sawadogo<sup>a</sup>, Richard Martel<sup>e</sup> ,  
Dorian Davarzani<sup>a</sup>, Azita Ahmadi-Sénichault<sup>b,c</sup> , Stéfan Colombano<sup>a</sup> 

<sup>a</sup> BRGM (French Geological Survey), Orléans 45060, France

<sup>b</sup> Univ. Bordeaux, CNRS, Bordeaux INP, I2 M, UMR 5295, F-33400, Talence, France

<sup>c</sup> Arts et Métiers Institute of Technology, CNRS, Bordeaux INP, Hesam Université, I2 M, UMR 5295, F-33400 Talence, France

<sup>d</sup> ADEME (French Environment and Energy Management Agency), Angers, 49004, France

<sup>e</sup> Centre Eau Terre Environnement, Institut national de la recherche scientifique (INRS), Québec, Canada

## ARTICLE INFO

### Keywords:

PEO  
DNAPL mobilization  
Non Newtonian fluid  
Heterogeneous aquifer  
Two-phase flow modeling

## ABSTRACT

Polymer solution injection has emerged as a promising method for the remediation of NAPL (non-aqueous phase liquids)-contaminated aquifers. This technique enhances recovery efficiency by modifying viscous forces, stabilizing the displacement front, and minimizing channeling effects. However, there remains a significant gap in understanding the behavior of polymer solutions, particularly those with different molecular weights (MW), for mobilizing DNAPL (dense non-aqueous phase liquids) trapped in heterogeneous aquifers, especially within low-permeability layers. In this study, we address this gap by investigating the mobilization of DNAPL lenses confined by low-permeability layers through the injection of polyethylene oxide (PEO) polymers of varying MW. PEO solutions with MW of 5 M (million) and 8 Mg/mol displayed shear-thinning behavior for shear rates of 0.01 to 100 s<sup>-1</sup>, while the 1 Mg/mol solution showed shear-thinning below 10 s<sup>-1</sup> and Newtonian behavior above. PEO solutions in porous media exhibit Newtonian behavior at low-to-moderate shear rates for all MWs, likely due to confinement-limited entanglement.

Adsorption studies found non-significant PEO adsorption on soil surfaces, likely due to its large molecular size. Post-flushing of PEO-saturated columns with water led to notable permeability reductions attributed to viscous fingering. Column tests indicated a decrease of the residual DNAPL saturation with the capillary number (Ca), more sharply in low permeability soils.

2D cell tests identified three stages of DNAPL mobilization: initial stabilization, sharp recovery increase upon PEO arrival, and a final stabilization at residual saturation. The duration of each transition was found to be influenced by concentration. Numerical simulations accurately mirrored these stages and provided additional insights into PEO viscosity distribution and DNAPL mobilization patterns in heterogeneous media. The results highlighted that higher injection rates promote mobilization from the two low permeability layers surrounding the DNAPL bank from both sides and the upper zone, while lower rates mainly drive mobilization from the upper side. Using numerical simulations the performance of PEO injection on displacement of DNAPL in multiple lenses and various position of recovery points was evaluated.

## 1. Introduction

Chlorinated organic hydrocarbons (COHs), hazardous contaminants in soils and groundwater, have become widespread due to extensive use and improper disposal. These solvents, forming dense non-aqueous phase liquids (DNAPLs), are denser and only slightly soluble in water, allowing them to migrate to significant depths, potentially reaching

impervious layer (Kueper et al., 2014). Initially, chlorinated solvent sites relied on pump-and-treat systems for remediation due to accessibility and ease of design. However, limitations emerged as contamination persisted, leading to a high cost per unit of removed contaminant (Kavanaugh et al., 2003). When DNAPL exists in subsurface pools, hydraulic displacement serves as an effective mass removal strategy for remediation (Alexandra et al., 2012). A key factor in developing this

\* Corresponding author.

E-mail address: [a.alamooti@brgm.fr](mailto:a.alamooti@brgm.fr) (A. Alamooti).

<https://doi.org/10.1016/j.watres.2024.122952>

Received 3 September 2024; Received in revised form 12 November 2024; Accepted 9 December 2024

Available online 12 December 2024

0043-1354/© 2024 The Author(s). Published by Elsevier Ltd. This is an open access article under the CC BY-NC license (<http://creativecommons.org/licenses/by-nc/4.0/>).

remediation approach is considering the heterogeneity of the contamination area. In contaminated heterogeneous geological formations, the use of shear-thinning fluids is essential to ensure that the displacing fluid does not bypass the targeted pollutants (Alamooti et al., 2023; Rodríguez de Castro et al., 2023).

Injecting non-Newtonian fluids during in situ remediation often leads to an enhanced recovery of pollutants. This improvement is achieved by increasing the viscosity of the fluid, which stabilizes the displacement front, minimizes channeling, and assists in displacing the contaminants more efficiently (Martel et al., 1998). Surfactant foam, as a specific example, has been widely used in the remediation of non-aqueous phase liquid (NAPL) contaminated aquifers. This method has been successfully tested and documented across various experimental setups, including micromodels (Jeong and Yavuz Corapcioglu, 2003), column studies (Fitzhenry et al., 2022; Liao et al., 2021; Longpré-Girard et al., 2020; Maire et al., 2018a, 2015; Omirbekov et al., 2020), 2D sandbox experiments (Longpré-Girard et al., 2016) and field scale applications (Hirasaki et al., 1997; Maire et al., 2018b). Although the surfactant foam can improve the mobilization of trapped NAPL, challenges arise in maintaining its stability and managing the elevated injection pressure (Omirbekov et al., 2020).

Heterogeneities in soils create preferential flow paths, reducing sweep efficiency and leaving significant non-swept areas in low-permeability zones (Grubb and Sitar, 1999). Viscous fingering occurs when a less viscous fluid displaces a more viscous resident fluid, destabilizing the flow. The key parameter, viscosity ratio ( $M_r$ : viscosity of displacing fluid/ viscosity of displaced fluid), determines sweep efficiency, with stable displacement occurring when  $M_r < 1$  (Martel et al., 2004). Water-soluble polymers, which are high molecular weight (MW) chemical agents exhibiting shear-thinning non-Newtonian behavior, can help mitigate fingering by increasing water viscosity, and improving sweep efficiency in heterogeneous soils (Martel et al., 1998). Martel et al. (1998) used a xanthan polymer solution for mobility control in NAPL-contaminated soil remediation within a multilayer system. They discovered that injecting the polymer solution post-surfactant alters mobility, enhancing it in low permeability zones. Martel et al. (2004) in a field scale study enhanced DNAPL displacement efficiency by sandwiching a micellar solution (comprising 12% Hostapur SAS surfactant, 12% n-butanol, 19% d-limonene, and 5% toluene) between preflush and postflush polymer (xanthan gum) slugs. The preflush polymer limited mobility and surfactant adsorption, while the postflush polymer pushed out the washing solution and improved front stability. Robert et al. (2006) achieved a 0.90 remediation factor

$\left( \frac{\text{volume of DNAPL recovered}}{\text{initial volume of DNAPL in porous media}} \right)$  for trichloroethylene (TCE) in a heterogeneous 2D sandbox by injecting a xanthan and surfactant mixture, effectively minimizing heterogeneity effects. Bouzid and Fatin-Rouge (2022) reached a remediation factor of 0.90 in 2D experiments by injecting a xanthan and sodium dodecyl sulfate (SDS) mixture into permeability-contrasted confined sandboxes with an egg-box shaped substratum. Alamooti et al. (2022) demonstrated, through experiments in a 2D sandbox of an unconfined DNAPL-saturated medium followed by numerical analysis, the critical need to counteract gravity forces during DNAPL displacement using a densified polymer suspension (Carboxymethyl cellulose as polymer and barite powder as densifier). In a follow-up experimental and numerical study, Alamooti et al. (2024a) investigated the performance of the injection of a densified polymer brine solution (xanthan as the polymer and NaI as water-soluble densifier) in both single-layer unconfined and multilayer confined 2D sandboxes, highlighting the importance of maintaining a near-zero gravity number to prevent density-driven flow issues. Omirbekov et al. (2023) explored the efficiency of injection of densified polymer suspension on displacement of DNAPL using column experiments. Alamooti et al. (2023) highlighted the performance of injecting a xanthan and SDBS (sodium dodecylbenzene sulfonate) surfactant solution in a multilayer DNAPL-saturated aquifer sandbox through both

experimental and numerical approaches. Moreover, Alamooti et al. (2024b) evaluated the effectiveness of post-injection treatments using an alcohol-surfactant-polymer mixture in a multilayer system to reduce DNAPL residual saturation in a multilayer aquifer. However, none of the studies addressed scenarios involving complex topologies where a DNAPL lens is sandwiched by low permeability layers. The behavior of polymers in complex geometries (like DNAPL lens is sandwiched by low permeability layers) has not been thoroughly studied in the literature. Such configurations represent a common DNAPL trapping mechanism in real-world situations (like paleo-channels at the interface between the aquifer and the aquitard), where pollutant transport through the subsurface stops upon encountering impermeable or low permeability barriers, unable to proceed due to the high threshold pressure required for penetration into these layers (Kueper et al., 2014).

PEO, a widely employed polymer consisting of ethylene oxide monomers, has a flexible random coil configuration and is commercially available in a wide range of MWs. It has been extensively used in enhanced oil recovery (EOR) industry (Gleasure and Phillips, 1990; Mejía et al., 2022; Trine et al., 2022). PEO's low toxicity and the abundance of ethylene oxide contribute to its popularity in common products like skin creams and toothpaste (Smyth Jr et al., 1970). PEO is a biodegradable, and biocompatible polymer, though its biodegradability depends on its molecular weight (Lei et al., 2022; Silva et al., 2018). After flushing the contaminated zone, the polymer can be further reduced by over-flushing with water to minimize its presence in the subsurface (Martel et al., 2004). Any residual polymer left in the soil can then undergo natural attenuation processes, facilitating gradual biodegradation. PEO, like other non-Newtonian polymers commonly used in soil remediation (e.g., xanthan gum and carboxymethyl cellulose), demonstrates shear-thinning behavior. However, unlike these biopolymers, PEO is available in a broader range of molecular weights, with its non-Newtonian properties influenced by both molecular weight and polymer concentration (Trine et al., 2022). Compared to xanthan, PEO requires higher concentrations to form thick solutions or gels (Basavaraju et al., 2007). Notably, to the best of our knowledge, PEO has yet to be utilized in soil remediation fields, where its shear-thinning behavior and environmentally friendly nature make it a promising candidate (Ebagninin et al., 2009).

In the framework of the PAPIRUS project, the remediation of a strongly heterogeneous aquifer contaminated with DNAPL is being studied through the injection of a polymer solution. The contaminated aquifer at the Tavaux site lies above a heterogeneous, undulating substratum with several paleo-channels. The main aim of this study is to explore the effect of injecting PEO solutions of varying MWs on the mobilization of DNAPL trapped by low permeable layers. Initially, we conducted a rheological analysis of PEO solutions across a range of MWs and concentrations. Subsequently, single-phase flow column experiments were undertaken to examine the adsorption of these solutions onto the soil particles' surfaces and to determine their apparent viscosity within porous media. Multiphase flow experiments in columns aimed to understand the performance of PEO solutions in displacing DNAPL in soils of differing permeabilities. Additionally, 2D cell experiments were conducted to closely mimic the conditions of real polluted sites and assess the performance of PEO solutions in mobilizing DNAPL. Specifically, we focused on the trapping of DNAPL in a highly permeable aquifer, surrounded by low-permeability layers, which closely replicates conditions at the Tavaux site. While the experimental model may seem idealized, it intentionally focuses on worst-case conditions where DNAPL is confined by low-permeability layers, which is a key aspect in challenging remediation efforts. A numerical model, integrating continuity and a generalized form of Darcy's law, was developed, and validated using experimental outcomes to simulate various injection scenarios.

The specific goals of this research include: (i) analyzing the rheological properties of PEO solutions with distinct MWs; (ii) comparing the efficiency of injecting PEO solutions with varying their MWs,

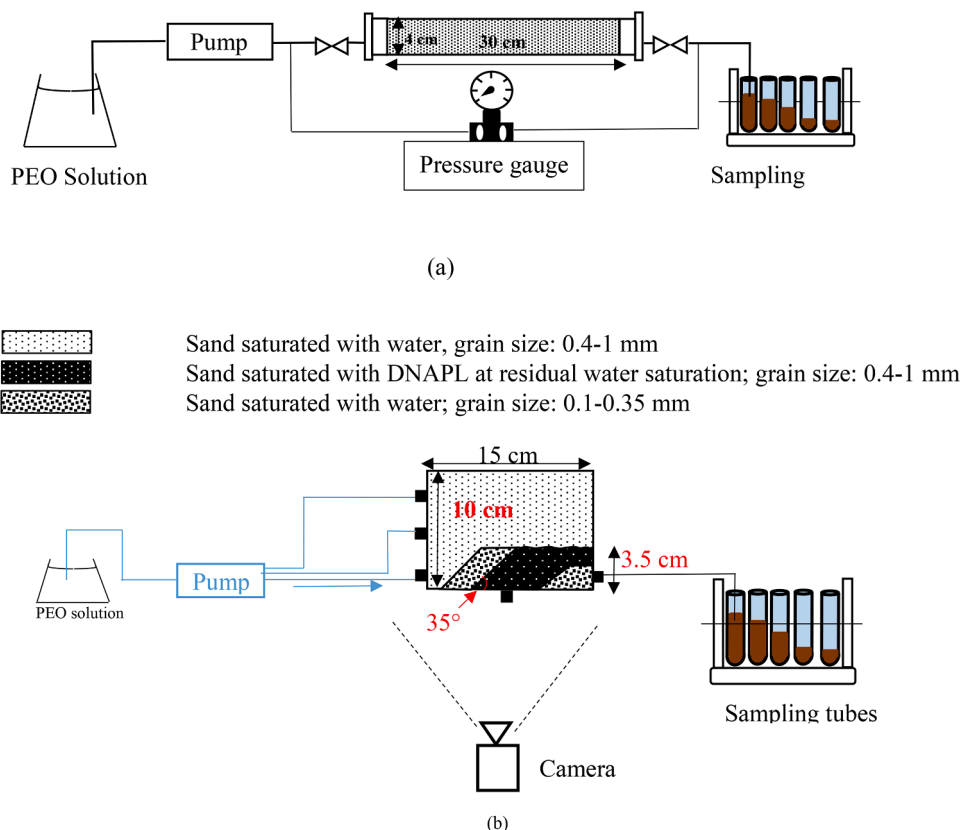


Fig. 1. Schematic of polymer-DNAPL displacement experimental setup: (a) 1D column setup, and (b) confined heterogeneous 2D aquifer cell.

concentrations, and densities, and injection velocities in mobilizing DNAPL trapped in a high permeable lens confined by two low permeable layers on each side; and (iii) employing multiphase flow modeling to have better insight into mechanisms of displacement, and to map the viscosity distribution within the porous media.

## 2. Materials and methods

### 2.1. Experimental materials

The porous media for these experiments consisted of packed beds of quartz sand, selected for its various particle-size fractions to represent different aquifer permeabilities. Specifically, we used fractions of 0.1–0.35 mm and 0.4–1 mm, corresponding to absolute permeabilities of  $29 \pm 2$  and  $199 \pm 15$  Darcy, respectively. The porosities for packing of fine and coarse sand have been found to be  $0.33 \pm 0.01$  and  $0.35 \pm 0.01$ , respectively. Each sand fraction was sieved, washed with deionized water, and oven-dried at  $105^\circ\text{C}$  for 10 h to ensure uniformity and remove impurities.

The multicomponent DNAPL chosen for this study was sourced from a contaminated site in Tavaux, France, with a composition primarily of hexachlorobutadiene (HCBd, 58%), hexachloroethane (HCA, 14%), penta-chlorobenzene (3.5%), and carbon tetrachloride (4%) (Colombano et al., 2021, 2020). This DNAPL mixture, exhibited a density of 1.66 g/mL and a viscosity of 4.47 mPa.s. Poly(oxyethylene) (POE), with the chemical formula  $\text{C}_{2n}\text{H}_{4n} + 2\text{O}_n + 1$ , was used as a water-soluble polymer in this study. It was selected in three different MWs of 1 million 1 M, 5 M, and 8 Mg/mol.

The POE for all specified MWs was purchased from Sigma-Aldrich. To analyze the rheological behavior of polymer solutions, we employed a Haake Mars 60 rotational rheometer with a cone-plate geometry. Additionally, the interfacial tension (IFT) between the polymer solutions and DNAPL was determined using a drop shape analyzer

apparatus (DSA-100, KRUSS) via the pendant drop method at an ambient temperature of  $22 \pm 1^\circ\text{C}$ . The total organic carbon (TOC) concentration in the effluent was quantified using a Shimadzu TOC analyzer, facilitating the determination of the polymer solution concentration.

### 2.2. Batch experiments (adsorption tests)

Batch experiments were conducted to examine the adsorption dynamics of PEO on sand surfaces. These experiments involved the preparation of 20 mL PEO solutions with concentration of 5 g/L using deionized water, which were then mixed with 10 g of fine sand in 50 mL polyethylene flasks. To ensure thorough mixing, a Gerhardt® LaboShake shaker was employed at 120 RPM, agitating the mixtures for various durations: 30 min, 2 h, 4 h, 12 h, 24 h, 48 h, and 72 h. Following agitation, the mixtures were centrifuged using a Sigma 3–30ks centrifuge at 10,000 RPM and  $20^\circ\text{C}$  for 10 min to facilitate the separation of the sand from the polymer solution. The concentration of PEO in the supernatant was then quantified using a TOC analyzer to assess the extent of polymer adsorption onto the sand.

### 2.3. 1D column and 2D aquifer cell experiments

Each glass column, measuring 4 cm in diameter and 30 cm in length was packed with uniform sand. The preparation phase involved  $\text{CO}_2$  flushing to remove trapped air, followed by saturation with degassed deionized water, ensuring consistent initial conditions for subsequent DNAPL and PEO solution injections. For the multiphase flow experiments, DNAPL was vertically injected from the bottom at a flow rate of 1 mL/min until residual water saturation was achieved, followed by a rotation and horizontal injection of PEO solutions with MWs of 1, 5, and 8 Mg/mol to assess their impact on DNAPL displacement. Effluent samples were collected in 15 mL propylene tubes, and both inlet and

**Table 1**  
Parameters used in displacement experiments.

Setup configuration (1D, 2D)	Concentration of PEO (g/L)	MW of PEO (Mg/mol)	Injection rate (mL/min)	Displaced phase	Sand Permeability ( $10^{-10} \text{ m}^2$ )	
1D column (D $4 \times L$ 30)	5	1	1	Water	1.99	
	5	5	1	water	1.99	
	5	8	1	water	1.99	
	5	1	1	Water	0.29	
	5	5	1	water	0.29	
	5	8	1	water	0.29	
	5	1	1	DNAPL	1.99	
	5	5	1	DNAPL	1.99	
	5	8	1	DNAPL	1.99	
	5	1	1	DNAPL	0.29	
	5	5	1	DNAPL	0.29	
	5	8	1	DNAPL	0.29	
	2D aquifer cell (L $15 \times H$ 10 $\times W$ 2)	5	1	$3 \times 0.33$	DNAPL/ water	Heterogeneous
		5	5	$3 \times 0.33$	DNAPL/ water	Heterogeneous
		5	8	$3 \times 0.33$	DNAPL/ water	Heterogeneous
10		5	$3 \times 0.33$	DNAPL/ water	Heterogeneous	
1		5	$3 \times 0.33$	DNAPL/ water	Heterogeneous	
5		5	$3 \times 0.66$	DNAPL/ water	Heterogeneous	
5		5	$3 \times 0.166$	DNAPL/ water	Heterogeneous	
5		5	$3 \times 0.33$	DNAPL/ water	Heterogeneous	
5		5	$3 \times 0.33$	DNAPL/ water	Heterogeneous	

outlet pressures were monitored using a pressure transducer (KELLER PR33X). In single-phase flow experiments, which were carried out for analysis of rheological behavior and transport of PEO polymers, PEO solutions with concentration of 5 g/L or a tracer (NaI solution with concentration of 4 g/L) were introduced into a fully water-saturated sand pack at a flow rate of 1 mL/min, and effluent samples were collected accordingly. The schematic of 1D column experimental setup is presented in Fig. 1a. Descriptive parameters for each experiment are detailed in Table 1. The concentration of PEO solutions used in the column experiments was set at 5 g/L to ensure stable flow, following Lenormand's criteria (Lenormand et al., 1988). This concentration also allowed for consistent comparison across different experimental cases.

A confined 2D aquifer cell, featuring dimensions of 15 cm  $\times$  10 cm  $\times$  2 cm with glass fronts for imaging, served as the experimental setup to assess the performance of injecting dyed PEO solutions into a heterogeneous system (Fig. 1b). The aquifer cell incorporated two low-permeability layers inclined at 35° at the bottom, sandwiching a high-permeability layer. The 3-layer structure is surrounded by a high permeable sand pack. The system was filled with sand under water, and DNAPL was introduced into the inclined high-permeability layer via the central port at the aquifer cell's bottom. Subsequently, PEO solutions were injected into the system through three ports on the left, while DNAPL recovery took place through the port on the right bottom.

Various experimental injection scenarios were designed, encompassing the injection of PEO solutions with MWs of 1, 5, and 8 Mg/mol at a concentration of 5 g/L, with an injection rate of  $3 \times 0.33$  mL/min. Additionally, injections included PEO solutions with MWs of 5 Mg/mol at concentrations of 1 g/L, 5 g/L, and 15 g/L, with an injection rate of  $3 \times 0.33$  mL/min. Further variations involved injections of PEO solutions with MWs of 5 Mg/mol at injection rates of  $3 \times 0.166$ ,  $3 \times 0.33$ , and  $3 \times 0.66$  mL/min, and injections of PEO solutions with MWs of 5 Mg/mol at injection rates of  $3 \times 0.33$  mL/min. Descriptive parameters for each experiment are detailed in Table 1.

#### 2.4. Numerical model

Generalized Darcy's law, combined with the mass conservation of each phase, can characterize multiphase flow in porous media at low Reynolds numbers (Bear, 2013):

$$\frac{\partial}{\partial t}(\phi \rho_i S_i) + \nabla \cdot (\rho_i \mathbf{u}_i) = 0 \text{ with } i = w, nw \quad (1)$$

$$\mathbf{u}_i = -\frac{k k_{ri}}{\mu_i} (\nabla p_i - \rho_i \mathbf{g}) \quad (2)$$

The subscripts "w" and "nw" correspond to the wetting and non-wetting phases, respectively. Porosity is denoted by the symbol  $\phi$  (-), time by  $t$  (s), and the density, saturation, and Darcy velocity of phase  $i$  are represented by  $\rho_i$  (kg/m<sup>3</sup>),  $S_i$  (-) and  $\mathbf{u}_i$  (m/s) respectively. Additionally,  $k$  (m<sup>2</sup>) signifies the scalar absolute permeability of the isotropic porous medium, and  $k_{ri}$  (-) represents the relative permeability for phase  $i$ . The viscosity and pressure of phase  $i$  are indicated by  $\mu_i$  (Pa s) and  $p_i$  (Pa) respectively, while the gravity vector is denoted by  $\mathbf{g}$  (m/s<sup>2</sup>).

The sum of the saturations is equal to one ( $S_w + S_{nw} = 1$ ), and the capillary pressure,  $p_c$  (Pa), is the pressure difference between non-wetting and wetting phases:

$$p_c(S_w) = p_{nw} - p_w \quad (3)$$

The capillary pressure, and the relative permeability curves within the model are depicted using Brooks and Corey functions (Brooks and Corey, 1964):

$$p_c = p_e \left( \frac{S_w - S_{wr}}{1 - S_{nwr} - S_{wr}} \right)^{-\frac{1}{\lambda}} \quad (4)$$

$$k_{rw} = k_{rw}^{max} \left( \frac{S_w - S_{wr}}{1 - S_{nwr} - S_{wr}} \right)^{\epsilon_w} \quad (5)$$

$$k_{rnw} = k_{rnw}^{max} \left( \frac{S_{nw} - S_{nwr}}{1 - S_{nwr} - S_{wr}} \right)^{\epsilon_{nw}} \quad (6)$$

The model incorporates  $\lambda$  (-) to represent the index of pore size distribution, with  $p_e$  symbolizing the entry pressure (Pa). The maximum relative permeability, or end points, for the wetting and non-wetting phases are denoted by  $k_{rw}^{max}$  and  $k_{rnw}^{max}$ , respectively. Saturation exponents for the wetting and non-wetting phases are indicated by  $\epsilon_w$  and  $\epsilon_{nw}$ , respectively. Furthermore,  $S_{wr}$  (-) and  $S_{nwr}$  (-) are used to represent the irreducible saturation for the wetting phase and the residual saturation for the non-wetting phase, respectively.

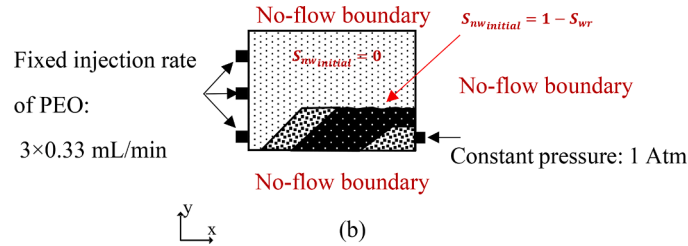
The advection-dispersion-reaction (ADR) equation describes the transport and fate of a solute, here the polymer, in a flowing fluid medium which is the wetting phase in this work:

$$\underbrace{\frac{\partial(\phi S_w c_i)}{\partial t}}_{\text{Accumulation}} = -\nabla \cdot (\mathbf{J}_{adv} + \mathbf{J}_{disp}) + \mathbf{R}_i \quad (7)$$

**Table 2**

Relative permeability and capillary pressure parameters obtained by inverse modeling and mean average error of experimental and numerical data for 2D aquifer cell.

Soil	$k_{rw}^{max}$	$k_{rnw}^{max}$	$\epsilon_w$	$\epsilon_{nw}$	$\lambda$	$p_c$ (Pa)	$S_{wr}$	$S_{nwr}$	MAE (Mean Absolute Error)
Low permeable	0.55	0.25	2	2.5	2	350	0.11	0.15	0.15
High permeable	0.6	0.4	2	2.6	2	200	0.09	0.07	

**Fig. 2.** Schematic of boundary and initial conditions for numerical simulations in 2D aquifer cell, 1 ml/min divide in 3 making 0.33 ML/min for each port.

where the concentration of the  $i$ -component ( $\text{kg/m}^3$ ) is represented by  $c_i$ , the reaction term for the  $i$ -component is indicated by  $R_i$  and  $J_{adv}$  and  $J_{disp}$  are advective and dispersive flux respectively:

$$J_{adv} = \mathbf{u}_w \cdot \mathbf{c}_i \quad (8)$$

$$J_{disp} = -\mathbf{D} \cdot \nabla \mathbf{c}_i \quad (9)$$

Where  $\mathbf{D}$  is the dispersion tensor and for two-dimensional systems can be expressed as (Bear, 2013):

$$\mathbf{D} = (\alpha_T |\mathbf{u}_w| + D_{eff}) \mathbf{I} + (\alpha_L - \alpha_T) \frac{u_{wx} u_{wy}}{|\mathbf{u}_w|} \quad (10)$$

$$D_{eff} = \frac{D_0}{\tau} \quad (11)$$

where  $\mathbf{I}$  denotes the identity matrix, while,  $u_{wx}$  and  $u_{wy}$  represent the wetting-phase velocity's longitudinal and transverse components, respectively. The terms  $\alpha_L$  and  $\alpha_T$  refer to the longitudinal and transverse dispersivities (m), respectively. The molecular diffusion coefficient is denoted by  $D_0$  ( $\text{m}^2/\text{s}$ ), and  $\tau$  signifies the tortuosity.

The simulation domain was discretized into 5141 triangular meshes. Eqs. (1) to (11) are discretized and simulated using COMSOL Multiphysics® with a MUMPS solver and quadratic interpolation for pressure. Table 2 details the key parameters such as relative permeability, and capillary pressure, obtained from inverse modeling of two-phase flow in a 2D aquifer cell. Their curves are demonstrated in Figure S1.

The maximum element growth rate was set to 1.2, with element sizes ranging from 0.00127 cm to 0.34 cm. A backward differentiation formula (BDF) was employed for time-stepping with a free time-stepping option. The boundary and initial conditions for the 2D aquifer cell, are shown in Fig. 2. To capture the effects of heterogeneity in the numerical model, two distinct homogeneous, isotropic, water-wet zones were defined: a high-permeability zone where DNAPL accumulates, and low-permeability layers that sandwich it. Each zone was assigned unique hydrogeological and flow properties, including permeability, porosity, relative permeability, and capillary pressures. These properties influence transport and flow within the heterogeneous system, as the low-permeability layers act as barriers, resisting flow and affecting DNAPL distribution.

### 3. Results and discussions

#### 3.1. Rheological analysis at bulk and porous media

Fig. 3a illustrates the rheological characteristics of PEO solutions

with MWs of 1, 5, and 8 Mg/mol, at concentrations of 5 and 10 g/L. These experiments have been triplicated, and error bars are calculated by determining the mean (average) of the data points and the standard deviation. The rheological behavior of PEO solution was described through the Cross fluid model (Cross, 1965) expressed as:

$$\mu = \mu_{inf} + \frac{(\mu_0 - \mu_{inf})}{(1 + (\chi \dot{\gamma})^l)} \quad (12)$$

where, the viscosities (Pa.s) at zero and infinite shear rate are denoted as  $\mu_0$  and  $\mu_{inf}$ ,  $\chi$  is the time constant (s), and  $l$  (-) is the power index. The parameters of Cross model for PEO solutions are shown in Table S1. Furthermore, Figure S2 depicts the rheological behavior of each MW individually (1, 5, and 8 Mg/mol) at different concentrations. Additionally, Fig. 3b overlays various viscosity-shear rate curves onto a master curve, achieved by plotting  $(\mu - \mu_{inf}) / (\mu_0 - \mu_{inf})$  as a function of the dimensionless shear rate  $(\chi \dot{\gamma})^l$ , utilizing parameters derived from the Cross model.

PEO solutions exhibit shear thinning due to less entanglement between polymer chains at higher shear rates. Lower MW PEO (1 Mg/mol) has fewer entanglements, leading to near-Newtonian behavior (Ebagnin et al., 2009). Similar to higher concentrations, higher MWs of PEO solutions (5 and 8 Mg/mol) form denser entanglement networks, resulting in higher viscosities. At low shear rates, these entanglements restrict chain movement, mimicking constant viscosity. As shear rate increases, the applied stress disrupts entanglements, allowing chain alignment and shear thinning behavior (Bahlouli et al., 2013; Ebagnin et al., 2009).

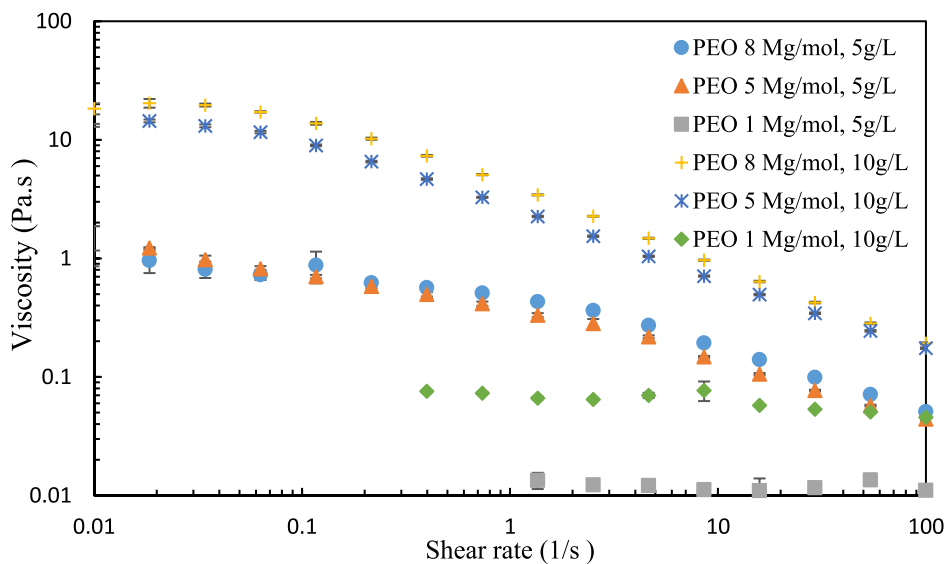
Through 1D column experiments, the apparent viscosity of 5 g/L PEO solutions in soils with two different permeabilities were investigated. The apparent shear rate within porous media at the Darcy scale can be described using the Darcy velocity as (Darby et al., 2017):

$$\dot{\gamma}_{app} = \sqrt{\frac{2}{\phi k}} u \quad (13)$$

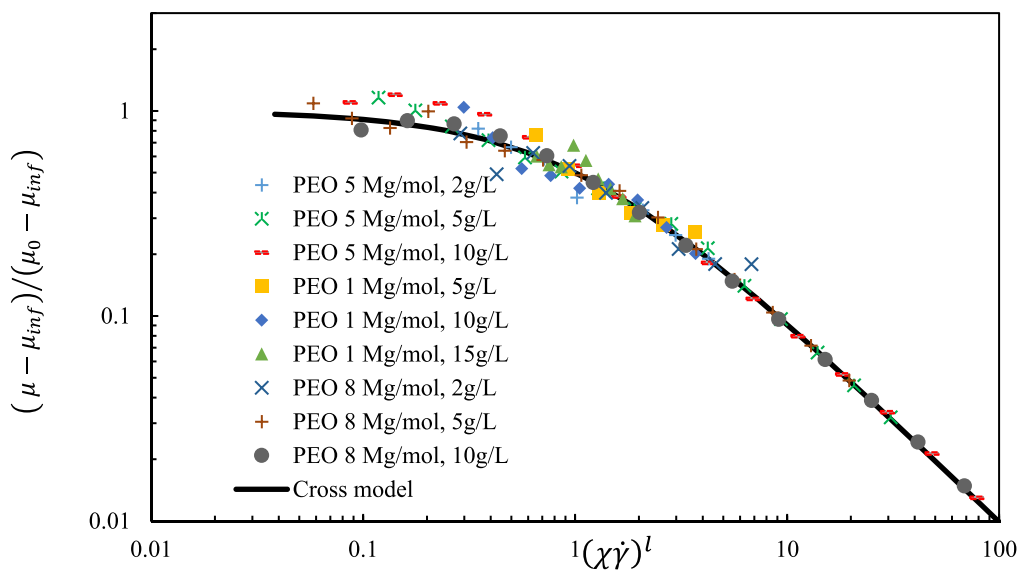
The resulting viscosity curves in porous media compared to those in bulk (fitted by Cross model) are shown in Fig. 4. Compared to bulk viscosity, a decrease in apparent viscosity was observed for higher MWs (5 & 8 Mg/mol). This reduction was more pronounced in the lower permeability media due to the depleted layer concept (Chauveteau and Zaitoun, 1981). Steric hindrance restricts the larger PEO molecules from approaching the pore walls, creating a thin depleted layer devoid of polymer molecules. This layer leads to a lower effective viscosity experienced by the flowing solution. The smaller pore size in the lower permeability media amplifies this effect. As the shear rate increases, the PEO molecules align with the flow direction, diminishing the difference between the apparent and bulk viscosity (Chauveteau and Zaitoun, 1981). The lower molecular weight PEO (1 Mg/mol) exhibited similar behavior in both media due to its smaller molecular size, allowing for unhindered movement within the pores and minimal impact on viscosity.

#### 3.2. PEO adsorption on soil particles

The process of measuring batch adsorption entails to put in contact soil particles with a polymer solution. The level of adsorption is quantified by comparing the polymer concentration before and after its



(a)



(b)

**Fig. 3.** Rheological behavior of PEO solutions with MWs of 1, 5 and 8 Mg/mol, (a) viscosity as a function of shear rate for concentrations of 5 and 10 g/L, (b) viscosity  $(\mu - \mu_{inf}) / (\mu_0 - \mu_{inf})$  as a function of the dimensionless shear rate  $(\chi\dot{\gamma})^l$ .

interaction with the soil particles. The batch experiments described in the previous section were conducted to evaluate the static adsorption of PEO on sand. Across all tested MWs and at a concentration of 5 g/L, there was no significant adsorption observed on the soil particles, as determined by TOC analysis, with a detection limit of 0.5%.

Column single-phase flow experiments were carried out to investigate adsorption under dynamic flow conditions. The findings, illustrated in Fig. 5, indicate that, similar to batch experiments, PEO particles do not significantly adsorb onto soil. This is evidenced by the breakthrough curves for both tracer and polymer solutions being similar, with breakthrough occurring approximately at 1 pore volumes injected (PV). PEO, being a neutral polymer (Mesbah et al., 2014) has minimized electrostatic interaction with negatively charged soil particles, and due

to the mineral nature of the soil, no significant hydrophobic interactions are expected. Additionally, PEO's large molecular size (Saigal et al., 2013) results in steric hindrance, which prevents close proximity to the pore walls. This creates a concentration gradient, with zero concentration at the pore walls and bulk concentration at a distance roughly equivalent to the polymer's macromolecular half-length. The steeper breakthrough of the PEO solutions (compared to the tracer) observed in Fig. 5 can be attributed to this steric hindrance, as larger molecules are less able to penetrate small pore spaces, leading to earlier appearance in the effluent. Furthermore, the high viscosity of the PEO solution compared to the tracer contributes to a more piston-like displacement, which explains the sharper breakthrough curve. It is important to note that these results are specific to the sandy soil used in this study, and

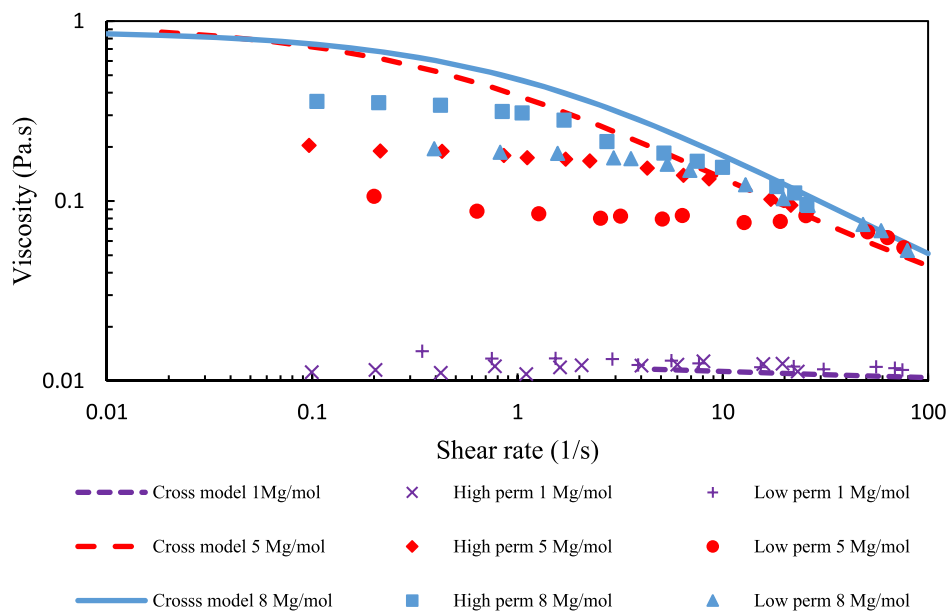


Fig. 4. Apparent viscosity of PEO solutions with different MWs at fixed concentration of 5 g/L in two different permeable porous media compared to the Cross model of their bulk viscosities.

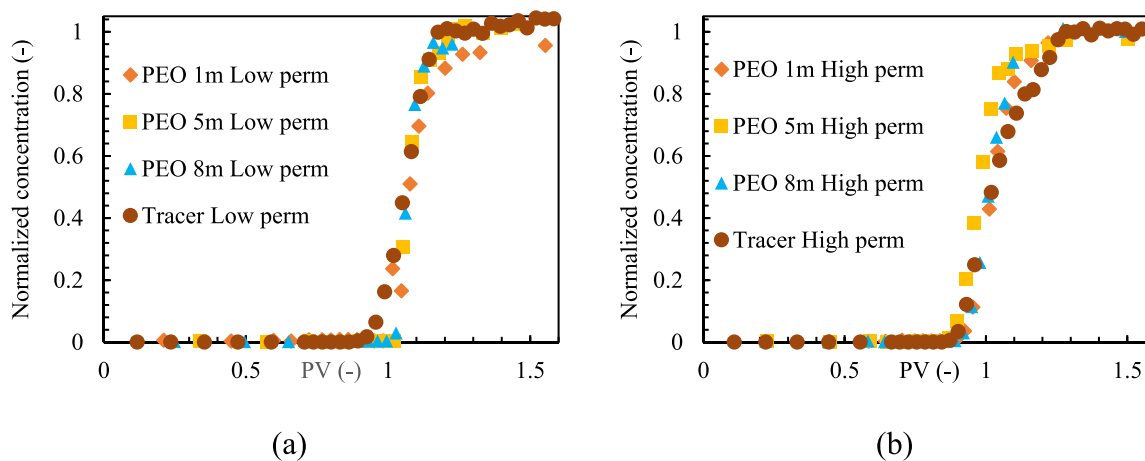


Fig. 5. Breakthrough curves for tracer, and PEO solutions in 1D columns. (a) Low permeable sand, and (b) High permeable sand.

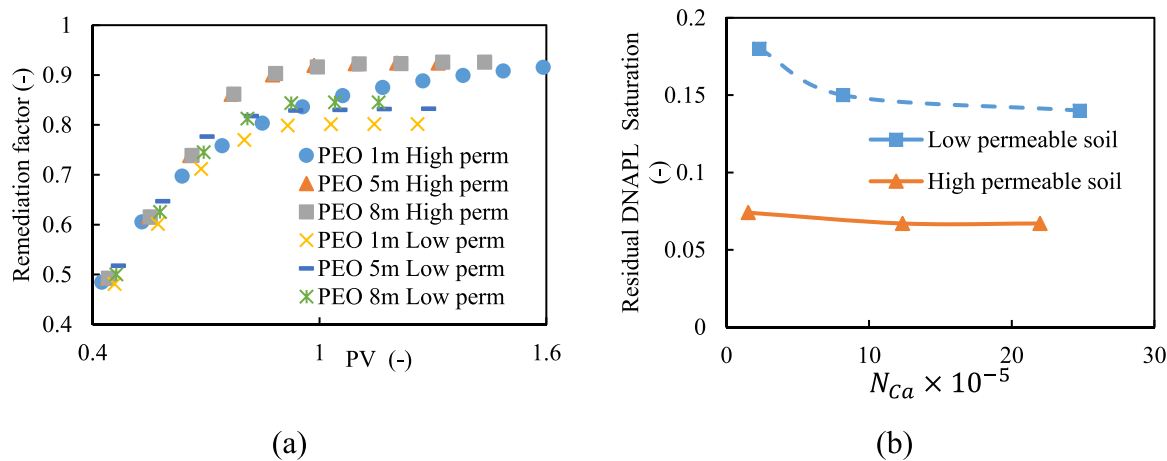
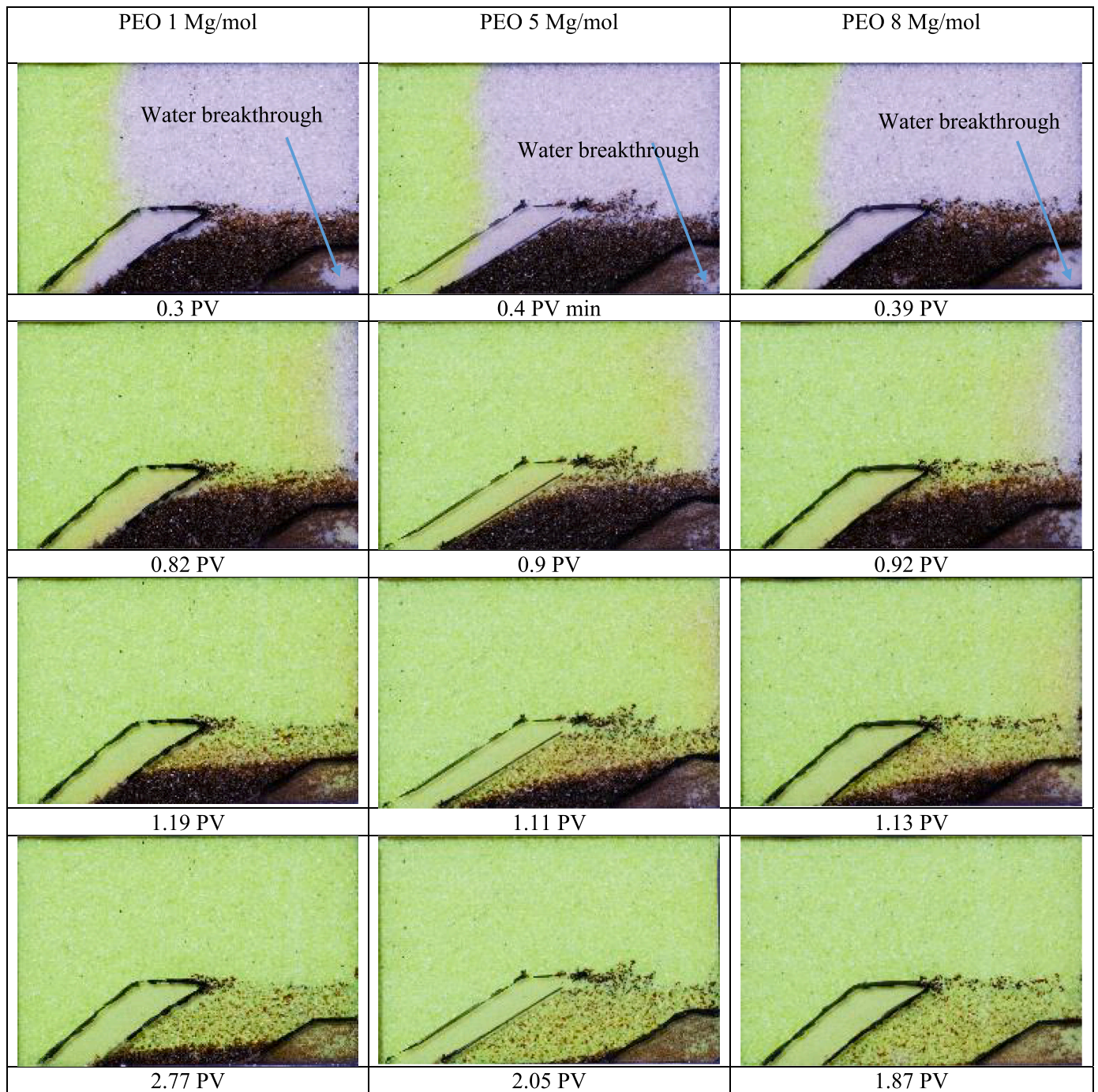


Fig. 6. Displacement of DNAPL in 1D column by PEO solutions: (a) remediation factor, (b) Residual DNAPL saturation versus capillary number.





**Fig. 7.** Dynamics of displacement of DNAPL in a high permeable layer sandwiched by two low permeable layers by injection of PEO solutions with different MWs, apparent viscosities of 0.012, 0.16, and 0.21 Pa.s and capillary numbers of  $7.72 \times 10^{-6}$ ,  $1.04 \times 10^{-4}$ ,  $1.3 \times 10^{-4}$  for 1, 5 and 8 Mg/mol respectively at a fixed concentration of 5 g/L, colors are green: PEO, grey: water; black: DNAPL.

further analysis is needed for soils containing other components, such as clay or organic matter.

However, the post-flushing of the polymer saturated columns by water shows a significant water permeability reduction for different MWs. For a highly permeable layer, the decrease in permeability is approximately 41%, 77%, and 79% for MWs of 1, 5, and 8 Mg/mol, respectively. In the case of a low permeability layer, the reduction in permeability is around 33%, 66%, and 71% for MWs of 1, 5, and 8 Mg/mol, respectively. These reductions in permeability can be attributed to the viscous fingering created by unfavorable mobility ratio during the water injection to flush the polymer solution in porous media. The

viscous PEO solution is partially bypassed in porous media and the final permeability is reduced. As the molecular weight increases, so does the viscosity, potentially leading to a greater degree of bypassing and consequently a more pronounced reduction in permeability.

### 3.3. Two-phase flow in 1D column

Fig. 6a shows the remediation factor and residual DNAPL saturation as a function of pore volumes injected (PV) into DNAPL-saturated columns for different PEO solutions with MWs of 1, 5, and 8 Mg/mol, and a fixed concentration of 5 g/L. The remediation factor increases with the

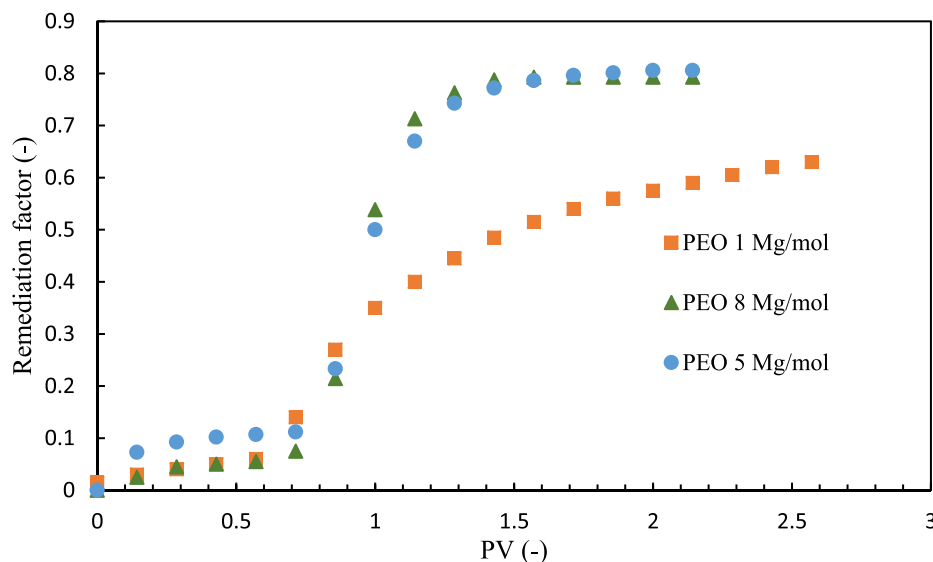


**Fig. 8.** Remediation factor curves for injection of PEO solutions at fixed concentration of 5 g/L with various MWs, apparent viscosities of 0.012, 0.16, and 0.21 Pa.s and capillary numbers of  $7.72 \times 10^{-6}$ ,  $1.04 \times 10^{-4}$ ,  $1.3 \times 10^{-4}$  for 1, 5 and 8 Mg/mol respectively into a 2D system composed of a DNAPL saturated high permeable soil sandwiched by two low permeable layers.

increasing number of pore volumes injected for all PEO solutions. PEO solutions with higher MWs (8 and 5 Mg/mol) show a greater remediation factor (around 0.1 more) compared to those with lower MW (1 Mg/mol).

The capillary number used to evaluate the performance of DNAPL production during the injection of the polymer solutions was calculated as (Chatzis and Morrow, 1984):

$$N_{ca} = \frac{k \Delta p}{\sigma L} \quad (14)$$

where  $\Delta p$  is the pressure difference along the column when the steady-state conditions has been achieved,  $L$  is the length of column  $\sigma$  (N/m) is the interfacial tension (IFT) between the DNAPL and solutions. The IFT between the PEO solutions and DNAPL was found around  $12.95 \pm 0.05$ ,  $13.39 \pm 0.05$  and  $13.62 \pm 0.05$  mN/m, for MWs of 1, 5, and 8 Mg/mol, respectively. The Fig. 6b presents capillary de-saturation curves for high and low permeable soils. The residual DNAPL saturation decreases with increasing capillary number for both low and high permeability soils.

### 3.4. DNAPL lens mobilization

Fig. 7 illustrates the dynamics of DNAPL mobilization from the highly permeable layer, sandwiched by lower permeability layers, upon the injection of PEO solutions of varying MWs at a fixed concentration of 5 g/L at different stages of injection (number of PVs injected). Initially, the injection of PEO solutions traverses the left less permeable layer and then causes DNAPL to migrate through the right less permeable layer due to the pressure drop near the recovery point. This flow stops once water from the surrounding area above the DNAPL zone (shown by an arrow in Fig. 7 at 0.4 PV) enters the low permeability layer. When the PEO solution (green in the figure) reaches the DNAPL zone (approximately at 0.9 PV), it displaces the entrapped DNAPL. Until this point, the displacement pattern remains consistent across different MWs. However, subsequent injection reveals that lower MW PEO (1 Mg/mol) leaves behind more DNAPL in the high permeability layer as it channels through the less permeable layers. In contrast, for higher MWs the viscous PEO solutions push out the remaining DNAPL more effectively.

This observation is further supported by the recovery curves (Fig. 8), which exhibit two distinct plateau phases. The initial plateau signifies the cessation of DNAPL recovery, attributed to the channeling of surrounding water through the low permeable layer following the natural

mobilization of DNAPL near the recovery point at the onset of injection. Subsequently, a rapid increase in remediation factor is observed, corresponding to the mobilization of DNAPL facilitated by the further invasion of PEO solutions into the contaminated zone. This increase in remediation factor stabilizes and reaches a secondary plateau for higher MW PEO solutions. However, in the case of 1 Mg/mol PEO, the increase in remediation factor is more gradual, and a secondary plateau is not achieved during the injection period of the experiment. The gradual increase in remediation recovery, along with the lower final recovery, is primarily due to the more favorable mobility ratio achieved with higher MW PEO compared to the 1 Mg/mol PEO.

### 3.5. Effect of concentration and injection rate

In two additional experimental series, the impacts of varying the concentration and the injection rate of 5 Mg/mol PEO were explored in the 2D cell. Fig. 9a presents the recovery curves for different concentrations of 5 Mg/mol PEO, indicating that alterations in concentration—which correlate to the viscosity of the PEO solutions (see Fig. 3)—do not affect the flow pattern up to the end of the initial plateau phase. This phase corresponds to a halt in DNAPL displacement, initially prompted by minor mobilization, followed by the channeling of the surrounding water. Nonetheless, upon the PEO solutions reaching the DNAPL zone, variations in DNAPL mobilization become apparent. Notably, a decrease in PEO concentration results in an extended transition zone between the two plateau phases, shown by arrows in Fig. 9a. This observation parallels the earlier analysis regarding the injection of PEO solutions with different MWs, where the mobility ratio, i.e., the viscosity variations in PEO solutions according to their concentrations, plays a significant role. The final remediation factor was 0.63 for a concentration of 2 g/L, whereas it was approximately 0.8 and 0.82 for concentrations of 5 g/L and 10 g/L, respectively, showing close values for the latter two concentrations.

Fig. 9b displays the recovery curves for injecting 5 Mg/mol PEO solutions at a concentration of 5 g/L and varying injection rates of 0.5, 1, and 4 mL/min, delivered equally through the three left ports of the 2D aquifer cell. The initial phase, typically marked by a plateau in recovery observed in previous experiments, shows slight differences. More precisely, DNAPL movement was gradually stabilized after the initial mobilization phase with the commencement of PEO injection at rates of 0.5 and 4 mL/min. Figure S3 illustrates the displacement patterns at

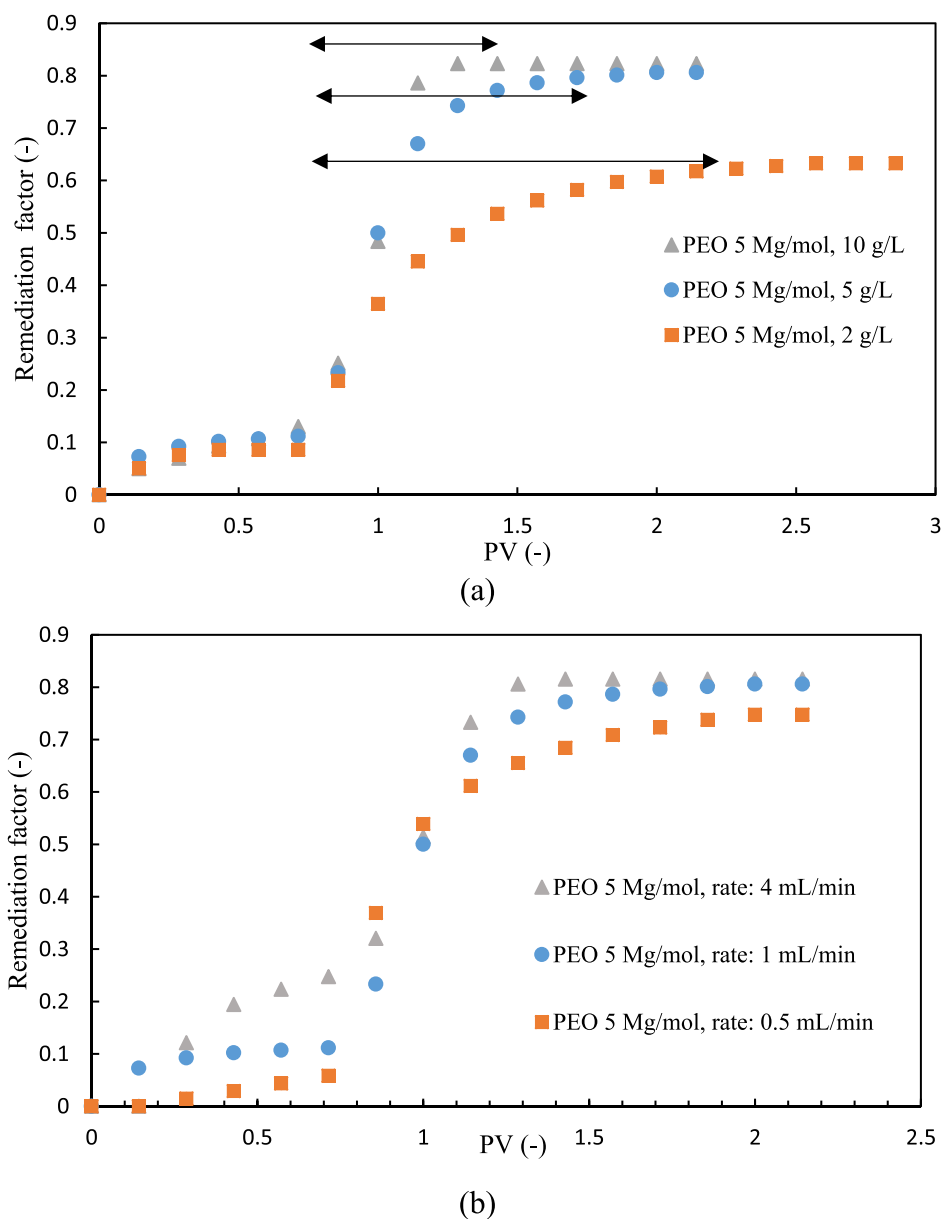
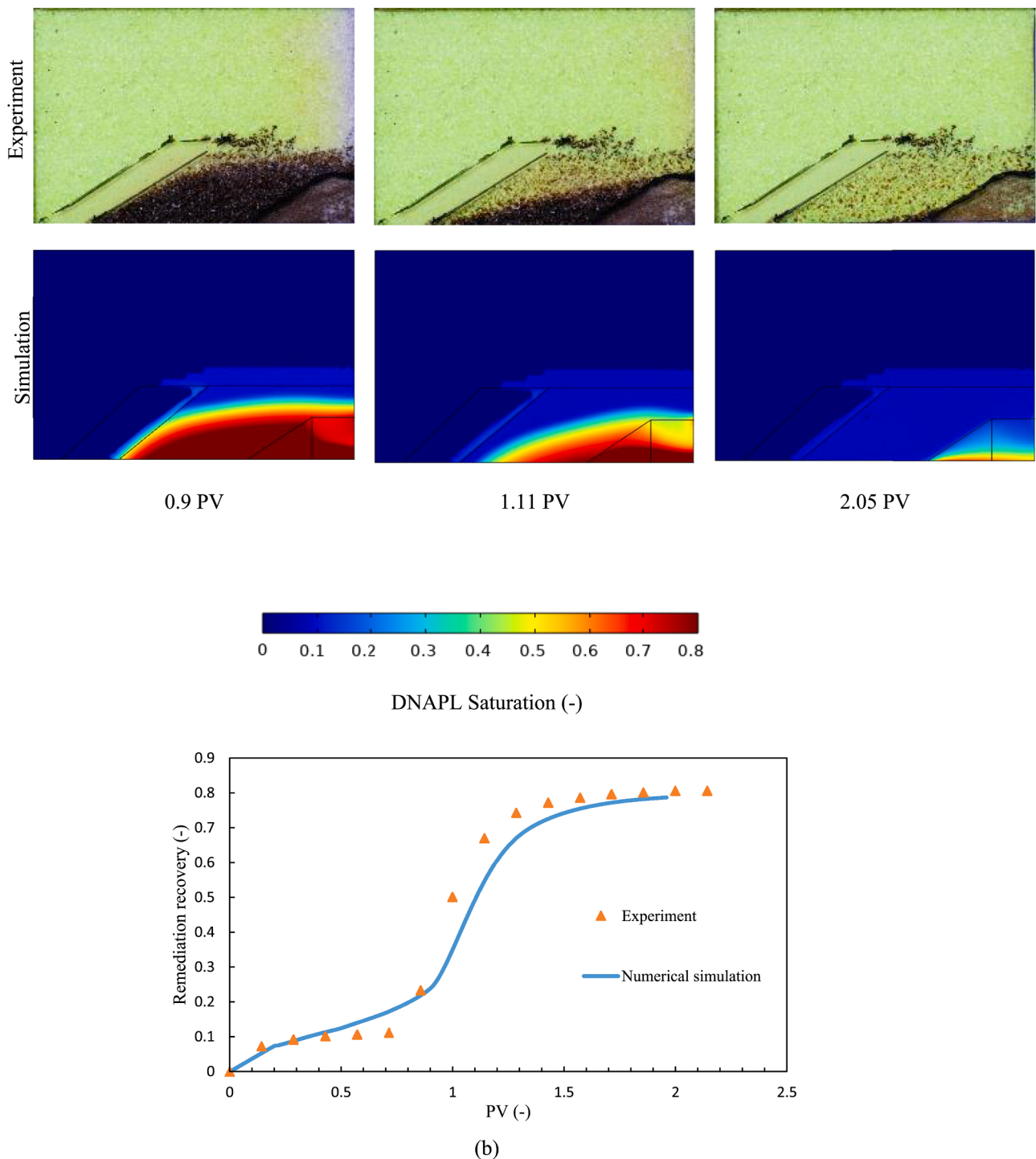


Fig. 9. Remediation factor curves for injection of PEO solutions with MW of 5 Mg/mol and with different (a) concentrations (arrows show extended transition zone between the two plateau phases), and (b) injection rates with apparent viscosities of 0.173, 0.167 and 0.132 Pa.s and capillary numbers of  $5.38 \times 10^{-5}$ ,  $1.04 \times 10^{-4}$ ,  $3.28 \times 10^{-4}$  for injection rates of 0.5, 1 and 4 mL/min.

different injection rates for 0.9 and 1.1 PVs, demonstrating that at higher injection rates, the PEO solution quickly mobilizes trapped DNAPL as soon as the left low-permeability layer is saturated with the polymer solution. Conversely, at lower injection rates, DNAPL mobilization beyond the initial phase only proceeds once both the upper high-permeability layer and the left low-permeability layer are saturated with the PEO solution. This pattern persists into later stages, with DNAPL being displaced more efficiently at the highest injection rate from the left section. This effect can be attributed to the greater pressure drop applied to the trapped DNAPL at higher injection rates, where viscous forces become more significant compared to capillary and gravity forces. At lower injection rates, the viscous forces are insufficiently strong to counteract the capillary forces. Simultaneously, the density difference between the polymer solution and DNAPL causes the PEO solution to occupy the upper parts of the DNAPL zone, with DNAPL mobilization resuming only after the upper region is completely saturated with the polymer solution.

### 3.6. Simulation of DNAPL mobilization and validation with experiments

To gain a deeper insight into the mechanisms governing DNAPL displacement and to characterize key parameters such as the apparent viscosity distribution of PEO solutions in heterogeneous porous media, numerical simulations were conducted. The results depicted in Fig. 10a demonstrate that the numerical model effectively replicates the experimental outcomes of PEO 5 Mg/mol injection at a concentration of 5 g/L and an injection rate of 1 mL/min. Furthermore, Fig. 10b presents a comparison of remediation factor curves between the experiment and numerical simulation. The distribution of PEO solution viscosity, modeled as a non-Newtonian fluid within the 2D aquifer cell, is illustrated in Figure S4. Notably, the viscosity of PEO is shown to be dependent on pressure drop, a relationship established through single-phase flow column experiments. Consequently, heterogeneities and distance from the injection point exert significant influence on viscosity. Specifically, lower permeability results in higher pressure drop and



**Fig. 10.** Comparison between the numerical and experimental results of DNAPL displacement by PEO 5 Mg/mol and injection rate of in a 2D system, (a) displacement pattern in which first row shows experimental results and second row the simulation results, and (b) remediation factor obtained from experiments and simulations.

consequently lower apparent PEO viscosity. Figure S5 compares the propagation of the polymer solution in the aquifer cell from both experimental and numerical simulations, demonstrating strong agreement between them.

To assess the impact of the recovery point location on DNAPL mobilization, an additional set of numerical simulations was conducted with PEO injection at a rate of  $3 \times 0.33$  mL/min, using PEO with a molecular weight of 5 Mg/mol. The recovery point was positioned adjacent to the high-permeability, DNAPL-saturated soil, as shown in

Figure S6a. As it can be seen in Figure S6b, shifting the recovery point position had a minor effect on the overall DNAPL mobilization pattern: rather than being displaced downward, the DNAPL shifted horizontally and upward as the PEO solution advanced toward the recovery point. Nonetheless, regardless of recovery point placement, the polymer injection effectively displaced DNAPL from the contaminated zone.

Experimental studies in the 2D aquifer cell have shown that at the highest injection rate, the DNAPL bank began to mobilize from both the upper side and the left side adjacent to the left low permeable layer.

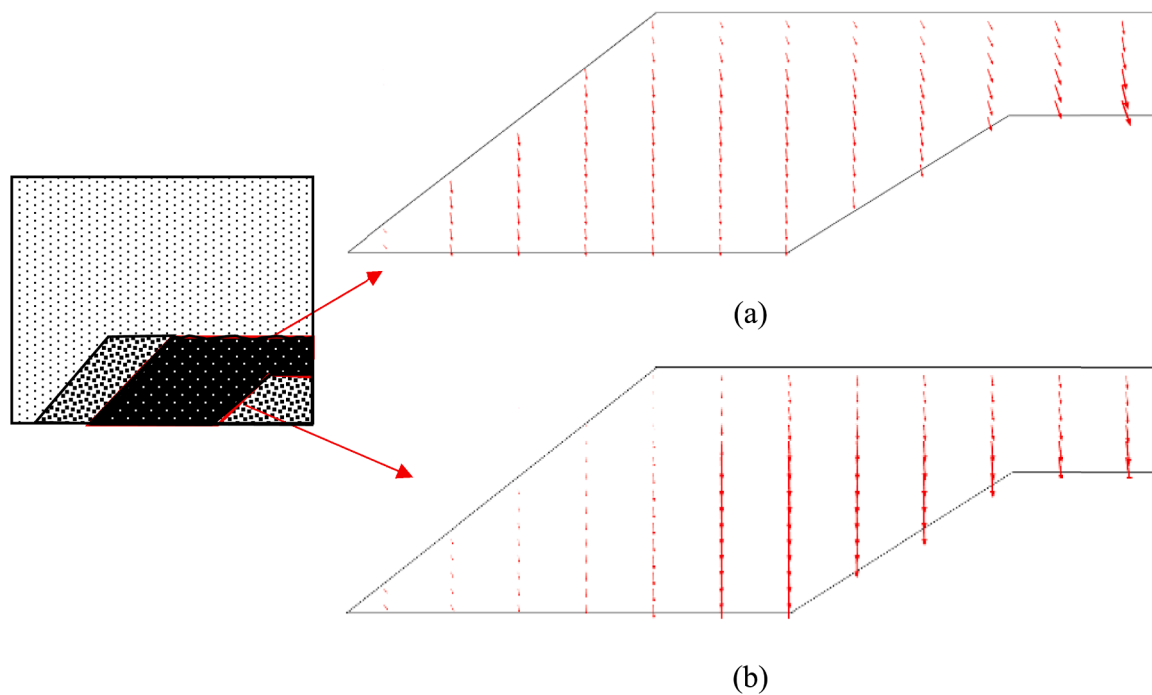


Fig. 11. Velocity field inside DNAPL saturated zone at 0.6 PV with injection rates of (a) 4 mL/min and (b) 1 mL/min.

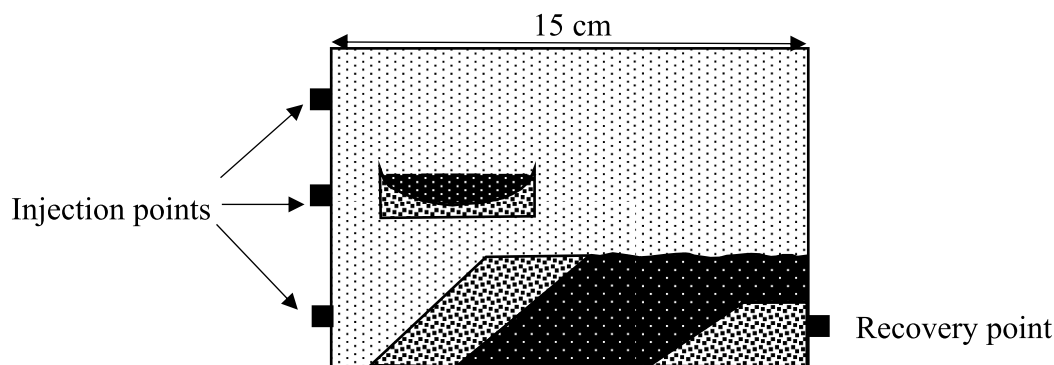
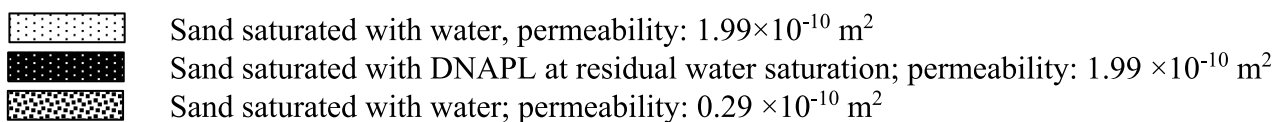


Fig. 12. Initial condition considered for the numerical simulation on complex DNAPL source zone architecture composed of multiple DNAPL lenses.

Numerical simulations were carried out at two different injection rates: 1 mL/min and 4 mL/min. The velocity field within the DNAPL-saturated zone at 0.6 pore volumes (PV) is illustrated in Fig. 11 with arrows proportional to the velocity magnitude. This visualization indicates that at the higher injection rate (4 mL/min, shown in 11a), flow occurs adjacent to both the left low permeable layer and the upper side of the DNAPL zone. In contrast, at the lower injection rate (1 mL/min, shown in 11b), flow predominantly occurs from the upper side, with limited flow from the left side.

### 3.7. Assessment of PEO injection on DNAPL mobilization in complex geological structure

In subsurface environments, DNAPL spatial distribution is described as the DNAPL source zone architecture, which depends on multiple parameters, including water-DNAPL interfacial tension, wettability, DNAPL density, geological structure and permeability, groundwater

velocity, spill volume, and duration (Kueper et al., 2014). Among these factors, the geological structure and permeability distribution play a significant role in DNAPL accumulation within the soil. To better understand PEO injection's efficiency in mobilizing DNAPL, a numerical simulation was conducted using a more complex geological model with multiple DNAPL lenses distributed in an aquifer, as illustrated in Fig. 12.

The scenario simulated involves an injection rate of  $3 \times 0.33 \text{ mL/min}$ , with a PEO solution of 5 Mg/mol MW at a concentration of 5 g/L. The results in Fig. 13(a-c) show that the DNAPL in the upper lens is mobilized only once the polymer solution reaches this contaminated area, after which it starts to mobilize downward toward the lower DNAPL lens due to gravity. In contrast, in this stage DNAPL in the lower lens undergoes limited mobilization because of preferential channeling of surrounding water, as this zone is near the recovery point. By the end of the displacement process, DNAPL in both zones is effectively displaced, however, in the upper lens it has partially penetrated the adjacent low-permeability zone, due to the flow direction toward the

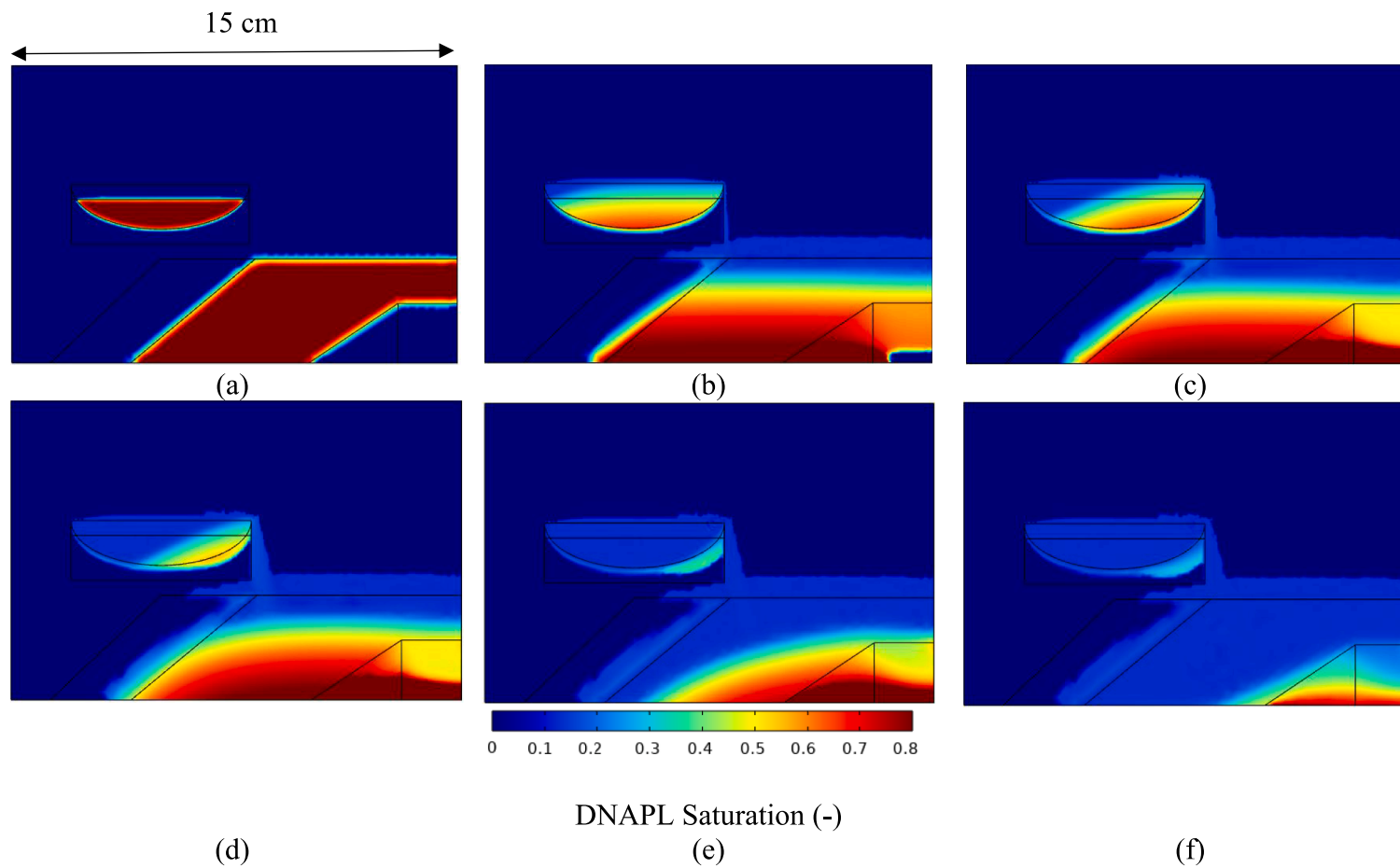


**Fig. 13.** DNAPL displacement pattern by injection of PEO at injection rate of  $3 \times 0.33$  mL/min, MW of 5 Mg/mol and at a concentration of 5 g/L in a complex multiple-lense system. (a) initial condition, (b) 30 min, (c) 60 min, (d) 90 min, (e) 120 min and (f) 200 min.

recovery point.

### 3.8. Implication of polymer injection at field scale

For the application of polymer injection in real-field remediation, several factors need to be considered for effective design and implementation. One of the primary concerns is optimizing the radius of influence of the polymer in the subsurface. This can be achieved through careful placement of both injection and recovery wells, considering their location and depth at the contaminated site (Giraud et al., 2018; Martel et al., 2004). The rates of injection and recovery also play a critical role, as they directly influence the radius of influence and control the flow patterns in the polluted zone. Given the shear-thinning behavior of polymers, continuous optimization of polymer concentration and polymer type are necessary to prevent blockages and maximize the radius of influence. Additionally, if the contamination is in an unconfined zone, confining the contaminated area could prevent density-driven issues, or the density of the injected polymer could be modified accordingly (Alamooti et al., 2024a, 2023).

Effective DNAPL remediation also requires accurate mapping of the contaminant plume and release dynamics. Non-invasive geophysical methods, such as Electrical Resistivity Tomography (ERT) and Induced Polarization (IP), hold significant potential for assessing DNAPL-contaminated sites and monitoring remediation efforts during and after treatment (Han et al., 2024; Koohbor et al., 2022).

In our ongoing work under the PAPIRUS project, we are conducting studies that include geophysical methods for evaluating and monitoring DNAPL mobilization in subsurface soils, and in future studies, we will further analyze the optimization of polymer injection conditions and assess their performance for field-scale applications.

## 4. Conclusions

A comprehensive series of experiments spanning various configurations, including bulk, column, and 2D aquifer cells, was conducted to evaluate the efficacy of injecting non-Newtonian PEO polymer solutions with different molecular weights and flow rates for displacing DNAPL banks sandwiched between two low permeable layers. Numerical simulations were performed and accurately predicted the experimental trends in the 2D cell.

Rheological analysis revealed non-Newtonian behavior for higher molecular weights (5 and 8 Mg/mol) of PEO, attributed to dense entanglement networks in their chains, while lower molecular weight (1 Mg/mol) PEO exhibited near-Newtonian behavior due to fewer entanglements. Observations in porous media indicated a decrease in apparent viscosity compared to bulk solutions, particularly for higher molecular weights, attributed to a depleted layer near pore walls resulting from steric hindrance of PEO molecules. Adsorption studies via batch and column experiments indicated negligible adsorption of PEO onto soil surfaces, likely due to the large molecular size. However, post-flushing of polymer-saturated columns with water revealed significant permeability reduction for different molecular weights, attributed to viscous fingering created by an unfavorable mobility ratio.

Two-phase flow experiments in columns demonstrated a decrease in residual DNAPL saturation with increasing capillary number for both low and high permeability soils, with a steeper decrease observed for low permeability soils. 2D aquifer cell tests delineated three stages of DNAPL mobilization between low permeable layers: an initial plateau in recovery due to DNAPL mobilization by pressure gradients near the recovery point, a sharp increase in recovery upon PEO arrival at the DNAPL zone, and a final plateau upon reaching residual DNAPL saturation. The effects of concentration and injection rates were also evaluated in 2D aquifer cell experiments. The lower the concentration, the longer is the transition zone between two plateaus (the second stage).

Numerical simulations, coupling mass conservation with the generalized Darcy law, effectively captured experimental outcomes of DNAPL

mobilization in the 2D system. These simulations elucidated the distribution of PEO solution apparent viscosity in heterogeneous porous media. Analysis of velocity fields in the DNAPL zone revealed that at higher injection rates, DNAPL mobilization occurs from both the left low permeable layer and upper side, whereas at lower injection rates, mobilization primarily results from PEO invasion from the upper side of the polluted zone. Using numerical simulations the performance of PEO injection on displacement of DNAPL in multiple lenses and various position of recovery points was evaluated. The laboratory results indicate that DNAPL recovery at heterogeneous sites depends on the interplay of viscous and gravity forces, the permeability contrast between geological units, and the mobility ratio of the injected fluids. Effective remediation requires optimizing these factors, particularly in low permeability zones, to enhance DNAPL mobilization and recovery.

## CRedit authorship contribution statement

**Amir Alamooti:** Writing – original draft, Visualization, Validation, Software, Methodology, Investigation, Formal analysis, Conceptualization. **Adil Baigadilov:** Methodology, Investigation, Data curation, Conceptualization. **Idriss Sawadogo:** Methodology, Investigation. **Richard Martel:** Writing – review & editing, Validation, Investigation. **Dorian Davarzani:** Writing – review & editing, Supervision. **Azita Ahmadi-Sénichault:** Writing – review & editing, Supervision, Investigation. **Stéfán Colombano:** Writing – review & editing, Supervision, Project administration, Funding acquisition, Conceptualization.

## Declaration of competing interest

The authors declare that they have no known competing financial interests or personal relationships that could have appeared to influence the work reported in this paper.

## Acknowledgments

This study was performed as part of the PAPIRUS project. The authors would like to thank ADEME (French Environment and Energy Management Agency) and BRGM for co-funding the project under the “GESIPOL” program and for providing the PhD grant for Amir Alamooti. The authors also gratefully acknowledge the financial support provided to the PIVOTS project by the “Région Centre – Val de Loire” and the European Regional Development Fund. We thank INEOS INOVYN for the assistance provided during the PAPIRUS project, in particular for providing access to the Tavaux site.

## Supplementary materials

Supplementary material associated with this article can be found, in the online version, at [doi:10.1016/j.watres.2024.122952](https://doi.org/10.1016/j.watres.2024.122952).

## Data availability

The data that has been used is confidential.

## References

- Alamooti, A., Colombano, S., Davarzani, D., Lion, F., Ahmadi-Sénichault, A., 2024a. Gravity-driven remediation of DNAPL polluted aquifers using densified biopolymer brine solution. *Adv. Water. Resour.*, 104643 <https://doi.org/10.1016/j.advwatres.2024.104643>.
- Alamooti, A., Colombano, S., Glabe, Z.A., Lion, F., Davarzani, D., Ahmadi-Sénichault, A., 2023. Remediation of multilayer soils contaminated by heavy chlorinated solvents using biopolymer-surfactant mixtures: two-dimensional flow experiments and simulations. *Water. Res.* 243, 120305. <https://doi.org/10.1016/j.watres.2023.120305>.
- Alamooti, A., Colombano, S., Omirbekov, S., Ahmadi, A., Lion, F., Davarzani, H., 2022. Influence of the injection of densified polymer suspension on the efficiency of DNAPL displacement in contaminated saturated soils. *J. Hazard. Mater.* 440, 129702. <https://doi.org/10.1016/j.jhazmat.2022.129702>.

- Alamootti, A., Colombano, S., Shoker, A., Ahmadi-Sénichault, A., Lion, F., Cazaux, D., Marion, C., Lagron, J., Sawadogo, I., Davarzani, D., 2024b. Enhancing remediation of residual DNAPL in multilayer aquifers: post-injection of alcohol-surfactant-polymer mixtures. *Sci. Total Environ.*, 170680 <https://doi.org/10.1016/j.scitotenv.2024.170680>.
- Alexandra, R., Gerhard, J.L., Kueper, B.H., 2012. Hydraulic displacement of dense nonaqueous phase liquids for source zone stabilization. *Groundwater* 50, 765–774.
- Bahloul, M.I., Bekkour, K., Benchabane, A., Hemar, Y., Nemdili, A., 2013. The effect of temperature on the rheological behavior of polyethylene oxide (PEO) solutions. *Applied Rheology* 23, 13435.
- Basavaraju, K.C., Demappa, T., Rai, S.K., 2007. Miscibility studies of polysaccharide Xanthan gum and PEO (polyethylene oxide) in dilute solution. *Carbohydr. Polym.* 69, 462–466. <https://doi.org/10.1016/j.carbpol.2007.01.004>.
- Bear, J., 2013. *Dynamics of Fluids in Porous Media*. Courier Corporation.
- Bouzhid, I., Fatin-Rouge, N., 2022. Assessment of shear-thinning fluids and strategies for enhanced in situ removal of heavy chlorinated compounds-DNAPLs in an anisotropic aquifer. *J. Hazard. Mater.* 432, 128703. <https://doi.org/10.1016/j.jhazmat.2022.128703>.
- Brooks, R.H., Corey, A.T., 1964. Hydraulic properties of porous media and their relation to drainage design. *Trans. ASAE* 7, 26–28.
- Chatzis, I., Morrow, N.R., 1984. Correlation of capillary number relationships for sandstone. *Soc. Petrol. Eng. J.* 24, 555–562. <https://doi.org/10.2118/10114-PA>.
- Chauveteau, G., Zaitoun, A., 1981. Basic rheological behavior of xanthan polysaccharide solutions in porous media: effects of pore size and polymer concentration. In: *Proceedings of the First European Symposium on Enhanced Oil Recovery*, Bournemouth, England, Society of Petroleum Engineers, Richardson, TX, pp. 197–212.
- Colombano, S., Davarzani, H., van Hullebusch, E.D., Huguenot, D., Guyonnet, D., Deparis, J., Ignatiadis, I., 2020. Thermal and chemical enhanced recovery of heavy chlorinated organic compounds in saturated porous media: 1D cell drainage-imbibition experiments. *Science of The Total Environment* 706, 135758. <https://doi.org/10.1016/j.scitotenv.2019.135758>.
- Colombano, S., Davarzani, H., van Hullebusch, E.D., Huguenot, D., Guyonnet, D., Deparis, J., Lion, F., Ignatiadis, I., 2021. Comparison of thermal and chemical enhanced recovery of DNAPL in saturated porous media: 2D tank pumping experiments and two-phase flow modelling. *Science of The Total Environment* 760, 143958. <https://doi.org/10.1016/j.scitotenv.2020.143958>.
- Cross, M.M., 1965. Rheology of non-Newtonian fluids: a new flow equation for pseudoplastic systems. *J. Colloid. Sci.* 20, 417–437.
- Darby, Ronald, Darby, Ron, Chhabra, R.P., 2017. *Chemical Engineering Fluid mechanics, Revised and Expanded*. CRC Press. <https://doi.org/10.1201/9781315274492>.
- Ebagninin, K.W., Benchabane, A., Bekkour, K., 2009. Rheological characterization of poly (ethylene oxide) solutions of different molecular weights. *J. Colloid. Interface Sci.* 336, 360–367.
- Fitzhenry, E., Martel, R., Robert, T., 2022. Foam injection for enhanced recovery of diesel fuel in soils: sand column tests monitored by CT scan imagery. *J. Hazard. Mater.* 434, 128777.
- Giraud, Q., Gonçalves, J., Paris, B., Joubert, A., Colombano, S., Cazaux, D., 2018. 3D numerical modelling of a pulsed pumping process of a large DNAPL pool: in situ pilot-scale case study of hexachlorobutadiene in a keyed enclosure. *J. Contam. Hydrol.* 214, 24–38. <https://doi.org/10.1016/j.jconhyd.2018.05.005>.
- Gleasure, R.W., Phillips, C.R., 1990. An experimental study of non-Newtonian polymer rheology effects on oil recovery and injectivity. *SPE reservoir engineering* 5, 481–486.
- Grubb, D.G., Sitar, N., 1999. Mobilization of trichloroethene (TCE) during ethanol flooding in uniform and layered sand packs under confined conditions. *Water. Resour. Res.* 35, 3275–3289. <https://doi.org/10.1029/1999WR900222>.
- Han, Z., Kang, X., Singha, K., Wu, J., Shi, X., 2024. Real-time monitoring of in situ chemical oxidation (ISCO) of dissolved TCE by integrating electrical resistivity tomography and reactive transport modeling. *Water. Res.* 252, 121195. <https://doi.org/10.1016/j.watres.2024.121195>.
- Hirasaki, G.J., Miller, C.A., Szafranski, R., Tanzil, D., Lawson, J.B., Meinardus, H., Jin, M., Londergan, J.T., Jackson, R.E., Pope, G.A., 1997. Field demonstration of the surfactant/foam process for aquifer remediation. In: *SPE Annual Technical Conference and Exhibition? SPE*, pp. SPE–39292.
- Jeong, S.-W., Yavuz Corapcioglu, M., 2003. A micromodel analysis of factors influencing NAPL removal by surfactant foam flooding. *J. Contam. Hydrol.* 60, 77–96. [https://doi.org/10.1016/S0169-7722\(02\)00054-2](https://doi.org/10.1016/S0169-7722(02)00054-2).
- Kavanaugh, M.C., Rao, P.S.C., Abriola, L., Cherry, J., Destouni, G., Falta, R., Major, D., Mercer, J., Newell, C., Sale, T., 2003. *The DNAPL Remediation challenge: Is there a Case For Source depletion?* US Environmental Protection Agency, National Risk Management Research.
- Koohbor, B., Deparis, J., Leroy, P., Ataie-Ashtiani, B., Davarzani, H., Colombano, S., 2022. DNAPL flow and complex electrical resistivity evolution in saturated porous media: a coupled numerical simulation. *J. Contam. Hydrol.* 248, 104003. <https://doi.org/10.1016/j.jconhyd.2022.104003>.
- Kueper, B.H., Stroo, H.F., Vogel, C.M., Ward, C.H., 2014. *Chlorinated Solvent Source Zone Remediation*. Springer.
- Lei, L., Bai, Y., Qin, X., Liu, J., Huang, W., Lv, Q., 2022. Current understanding of hydrogel for drug release and tissue engineering. *Gels* 8, 301.
- Lenormand, R., Touboul, E., Zarcone, C., 1988. Numerical models and experiments on immiscible displacements in porous media. *J. Fluid. Mech.* 189, 165–187. <https://doi.org/10.1017/S0022112088000953>.
- Liao, S., Saleeba, Z., Bryant, J.D., Abriola, L.M., Pennell, K.D., 2021. Influence of aqueous film forming foams on the solubility and mobilization of non-aqueous phase liquid contaminants in quartz sands. *Water. Res.* 195, 116975. <https://doi.org/10.1016/j.watres.2021.116975>.
- Longpré-Girard, M., Martel, R., Robert, T., Lefebvre, R., Lauzon, J.-M., 2016. 2D sandbox experiments of surfactant foams for mobility control and enhanced LNAPL recovery in layered soils. *J. Contam. Hydrol.* 193, 63–73. <https://doi.org/10.1016/j.jconhyd.2016.09.001>.
- Longpré-Girard, M., Martel, R., Robert, T., Lefebvre, R., Lauzon, J.-M., Thomson, N., 2020. Surfactant foam selection for enhanced light non-aqueous phase liquids (LNAPL) recovery in contaminated aquifers. *Transp. Porous. Media* 131, 65–84.
- Maire, J., Coyer, A., Fatin-Rouge, N., 2015. Surfactant foam technology for in situ removal of heavy chlorinated compounds-DNAPLs. *J. Hazard. Mater.* 299, 630–638. <https://doi.org/10.1016/j.jhazmat.2015.07.071>.
- Maire, J., Joubert, A., Kaifas, D., Invernizzi, T., Marduel, J., Colombano, S., Cazaux, D., Marion, C., Klein, P.-Y., Dumestre, A., Fatin-Rouge, N., 2018a. Assessment of flushing methods for the removal of heavy chlorinated compounds DNAPL in an alluvial aquifer. *Science of The Total Environment* 612, 1149–1158. <https://doi.org/10.1016/j.scitotenv.2017.08.309>.
- Maire, J., Joubert, A., Kaifas, D., Invernizzi, T., Marduel, J., Colombano, S., Cazaux, D., Marion, C., Klein, P.-Y., Dumestre, A., Fatin-Rouge, N., 2018b. Assessment of flushing methods for the removal of heavy chlorinated compounds DNAPL in an alluvial aquifer. *Science of The Total Environment* 612, 1149–1158. <https://doi.org/10.1016/j.scitotenv.2017.08.309>.
- Martel, K.E., Martel, R., Lefebvre, R., Gélinas, P.J., 1998. Laboratory study of polymer solutions used for mobility control during in situ NAPL recovery. *Ground. Water. Monit. Remediat.* 18, 103–113. <https://doi.org/10.1111/j.1745-6592.1998.tb00734.x>.
- Martel, R., Hébert, A., Lefebvre, R., Gélinas, P., Gabriel, U., 2004. Displacement and sweep efficiencies in a DNAPL recovery test using micellar and polymer solutions injected in a five-spot pattern. *J. Contam. Hydrol.* 75, 1–29. <https://doi.org/10.1016/j.jconhyd.2004.03.007>.
- Mejía, M., Pope, G.A., Song, H., Balhoff, M.T., 2022. Experimental Investigation of Polyethylene Oxide Polymer Solutions for Enhanced Oil Recovery in Low-Permeability Carbonate Rocks. *SPE Journal* 27, 929–944.
- Mesbah, K., Verpillot, R., Chiari, M., Pallandre, A., Taverna, M., 2014. Neutral polymers as coatings for high resolution electrophoretic separation of A $\beta$  peptides on glass microchips. *Analyst* 139, 6547–6555.
- Omirebekov, S., Colombano, S., Alamootti, A., Batikh, A., Cochenec, M., Amanbek, Y., Ahmadi-Sénichault, A., Davarzani, H., 2023. Experimental study of DNAPL displacement by a new densified polymer solution and upscaling problems of aqueous polymer flow in porous media. *J. Contam. Hydrol.* 252, 104120. <https://doi.org/10.1016/j.jconhyd.2022.104120>.
- Omirebekov, S., Davarzani, H., Ahmadi-Sénichault, A., 2020. Experimental Study of Non-Newtonian Behavior of Foam Flow in Highly Permeable Porous Media. *Ind. Eng. Chem. Res.* 59, 12568–12579. <https://doi.org/10.1021/acs.iecr.0c00879>.
- Robert, T., Martel, R., Conrad, S.H., Lefebvre, R., Gabriel, U., 2006. Visualization of TCE recovery mechanisms using surfactant-polymer solutions in a two-dimensional heterogeneous sand model. *J. Contam. Hydrol.* 86, 3–31. <https://doi.org/10.1016/j.jconhyd.2006.02.013>.
- Rodríguez de Castro, A., Ben Abdelwahed, A., Bertin, H., 2023. Enhancing pollutant removal from contaminated soils using yield stress fluids as selective blocking agents. *J. Contam. Hydrol.* 255, 104142. <https://doi.org/10.1016/j.jconhyd.2023.104142>.
- Saigal, T., Riley, J.K., Golas, P.L., Bodvik, R., Claesson, P.M., Matyjaszewski, K., Tilton, R. D., 2013. Poly (ethylene oxide) star polymer adsorption at the silica/aqueous interface and displacement by linear poly (ethylene oxide). *Langmuir* 29, 3999–4007.
- Silva, T.L.da, Araujo, F.P.de, Silva, E.C.da, Furtini, M.B., Osajima, J.A., 2018. Degradation of poly (ethylene oxide) films using crystal violet. *Materials Research* 20, 869–872.
- Smyth Jr, H.F., Weil, C.S., Woodside, M.D., Knaak, J.B., Sullivan, L.J., Carpenter, C.P., 1970. Experimental toxicity of a high molecular weight poly (ethylene oxide). *Toxicol. Appl. Pharmacol.* 16, 442–445.
- Trine, E.B., Pope, G.A., Britton, C.J., Dean, R.M., Driver, J.W., 2022. Novel Application of Polyethylene Oxide Polymer for EOR from Oil-Wet Carbonates. In: *SPE Improved Oil Recovery Conference? SPE*. D031S037R001.